

Article

High Gas Response Performance Based on Reduced Graphene Oxide/SnO₂ Nanowires Heterostructure for Triethylamine Detection

Ruiqin Peng¹, Xuzhen Zhuang¹, Yuanyuan Li², Zhiguo Yu¹ and Lijie Ci^{2,*} ¹ School of Intelligence Engineering, Shandong Management University, Jinan 250357, China² School of Materials Science and Engineering, Harbin Institute of Technology (Shenzhen), Shenzhen 518055, China

* Correspondence: cilijie@hit.edu.cn

Abstract: SnO₂ nanowires are locally synthesized by a simple thermal evaporation method and its growth mechanism is confirmed. Here, we present a simple strategy for realizing reduced graphene oxide (RGO)/SnO₂ nanowires heterostructure. As expected, the heterostructure gas-sensing response is up to 63.3 when the gas concentration of trimethylamine (TEA) is 50 ppm, and it exhibits an excellent dynamic response with high stability at 180 °C. A low detection limit of 50 ppb level is fully realized. Compared to SnO₂ nanowires, the sensing performance of the RGO/SnO₂ heterostructure-based sensor is greatly enhanced, which can be ascribed to the RGO and the heterostructure. The RGO/SnO₂ composite engineering poses an easy way to make full use of the advantages originating from RGO and heterostructure.

Keywords: RGO/SnO₂; heterostructure; gas response; mechanism



Citation: Peng, R.; Zhuang, X.; Li, Y.; Yu, Z.; Ci, L. High Gas Response Performance Based on Reduced Graphene Oxide/SnO₂ Nanowires Heterostructure for Triethylamine Detection. *Coatings* **2023**, *13*, 849. <https://doi.org/10.3390/coatings13050849>

Academic Editor: Keith J. Stine

Received: 28 March 2023

Revised: 24 April 2023

Accepted: 27 April 2023

Published: 29 April 2023



Copyright: © 2023 by the authors. Licensee MDPI, Basel, Switzerland. This article is an open access article distributed under the terms and conditions of the Creative Commons Attribution (CC BY) license (<https://creativecommons.org/licenses/by/4.0/>).

1. Introduction

Owing to the great demands of the chemical industry and real-time gas monitoring systems, high sensitivity and good stability of gas sensors are attracting tremendous attention. SnO₂, ZnO, and WO₃ have always been the traditional and dominant materials for sensor fabrication [1–6]. However, the excellent stability, long-cycles, and low detection limit of the sensors still face the challenge, especially working at a high temperature above 200 °C. At higher temperatures, the inevitable grain growth of materials would degrade the sensor stability and life [6]. Researchers have tried to implement some strategies (e.g., low dimensional nanostructures, metal doping, heterostructure engineering, etc.) for enhancing gas-sensing properties [7–9]. One-dimensional SnO₂ nanowire has a large surface-to-volume ratio and constant carrier screening length, which makes them more sensitive and efficient than SnO₂ film to transduce surface chemical processes into electrical signals [10]. Zou et al. demonstrated a hollow SnO₂ microfiber as a sensing layer and found a high response to TEA gas. However, the optimal operating temperature is up to 270 °C [11].

As a promising sensing material and derivative material of the graphene family, the RGO layer can provide more adopted active sites and fast gas diffusion. It normally acts as a p-type semiconductor, exhibiting the unique advantages of gas sensitive at room temperature [12]. Therefore, it has exhibited great potential for enhancing sensor performance by combing the merits of the one-dimensional SnO₂ nanowire and RGO material. For example, Song et al., reported a sensitive SnO₂/RGO nanocomposite H₂S gas sensor and the optimal sensor response was 33 in 2 s at 50 ppm of H₂S, which showed great potential in application [13]. Zhang et al. presented the synthesis of Ag/SnO₂/RGO ternary nanocomposites, and the composite sensors exhibited high response to TEA gas at 220 °C [14]. However,

RGO/SnO₂ crystalline nanowires composite gas sensors for TEA detection have been reported very little.

Here, we reported on the RGO/SnO₂ nanowires composite heterostructure for TEA gas sensing, which fully integrated the advantages of the RGO and SnO₂ nanowire by forming RGO/SnO₂ heterostructure and enhanced the gas-sensing properties. When the concentration of TEA gas was 50 ppm, the response was up to 63.3 and it exhibited good stability. The sensors were more sensitive to TEA gas than other gases. The sensing performance of the RGO/SnO₂ nanowires composite heterostructure is enhanced compared to that of SnO₂ nanowires; the mechanism is also discussed.

2. Materials and Methods

2.1. Preparation of RGO/SnO₂ Nanowires Composite Heterostructure

Synthesis of RGO. Graphene oxide (GO) water dispersion was purchased from Suzhou Tanfeng Graphene Tech. Inc. (Suzhou, China) The GO (1 mg/25 mL) was reduced into RGO by a chemically reducing method [15]. Briefly, the Hydroxylamine Hydrochloride (0.2 g) was added into the GO dispersion. The mixture was stirred for 6 h and then was under ultrasonic treatment for 1 h. After that, the dispersions were transferred into a 50 mL Teflon-lined stainless steel autoclave and maintained at 100 °C for 12 h. The black product was filtered and rinsed by acetone, ethanol, and deionized water to obtain the pure RGO powder.

Fabrication of SnO₂ nanowires and sensors. The SnO₂ nanowires were prepared by thermal evaporation method. The SnO₂ nanowires are fabricated using the above procedures as shown in Figure 1a, which shows the growth conditions of SnO₂ nanowires. Firstly, Sn powder was placed on the quartz plate, and SiO₂/Si substrates (1 × 1 cm²) with Au film (5 nm) were placed about 5 cm away from the Sn powder. Then, we placed the quartz piece in the center of the tube furnace. Ar gas (20 standard cubic centimeter per minute (sccm)) was introduced into the tube and the furnace pressure was constant at about 100 Pa. The furnace temperature was raised to 1000 °C by 10 °C/min. The nanowires growth period was about 20 min. The Au film pattern staying on the substrate was confined by the standard lithography process. The interdigitated Au-film electrode of the sensors was a planar device structure and the thickness was about 200 nm. Then, the RGO powder was fully dispersed in N, N-dimethylformamide (DMF) (0.5 mg/mL) by ultrasonication treatment for 2 h and was coated onto the surface of SnO₂ nanowires by spinning coating. Afterward, the samples were dried in vacuum oven at 60 °C for 4 h and then annealed at 200 °C for 60 min under Ar atmosphere to remove residual DMF. Finally, gas sensors were aged at 120 °C for 24 h. Figure 1b details the fabricating processes of RGO/SnO₂ composite-based sensor.

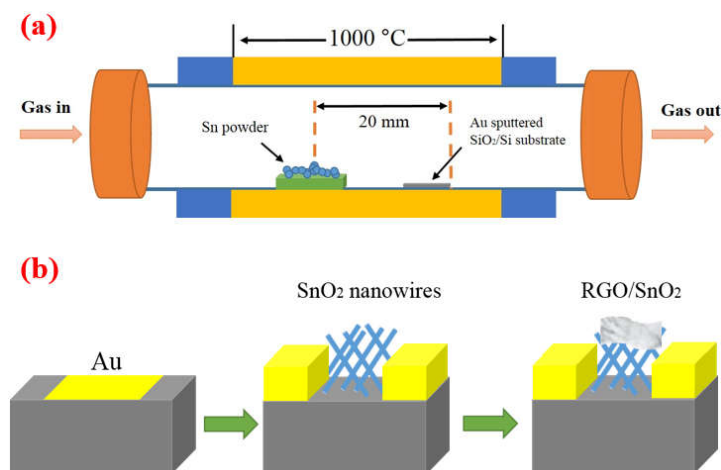


Figure 1. (a) Schematic of the synthesizing process of the SnO₂ nanowires; (b) the RGO/SnO₂ composite heterostructure-based sensor preparation process.

2.2. Materials Characterization and Sensor Properties

The microstructure and morphology were characterized by the FEI QUANTA 200 scanning electron microscope (SEM, FEI, Hillsboro, OR, America). The transmission electron microscope (TEM, JEM-2100, JEOL, Tokyo, Japan) with the selected area electron diffraction (SAED) and energy-dispersive X-ray spectroscopy (EDS). The crystalline structure was identified by MiniFlex 600 X-ray powder diffraction (XRD, Rigaku, Tokyo, Japan) with Cu $K\alpha_1$ radiation ($\lambda = 1.54056 \text{ \AA}$). The surface chemistries were identified by Raman spectrometer (LabRAM HR800, Horbiba Jobin Yvon, Paris, France). The gas-sensing properties were tested using a commercial CGS-4TP analysis system. The test system has a closed chamber with a capacity of 18 L. The TEA solution was injected and was heated as gas molecular transport to the surface of the sensor. The gas response was defined as using the ratio of the sensor resistance in air (R_a) to that in the target gas (R_g). The sensing properties were tested at temperatures from 25 to 250 °C. The response and recovery time were calculated as 90% of the maximum after injecting target gas and backing to air [16]. The relative humidity was kept constant at 50%~60%.

3. Results and Discussion

Figure 2 shows the morphology and microstructure of the RGO/SnO₂ composite. In Figure 2a,b, the RGO layer adhered onto the surface of SnO₂ nanowires. The nanowires are long and straight. The diameter of the nanowire is around 50 nm and the length is up to 50 μm . The existing network structure of SnO₂ nanowires gets a large surface-to-volume ratio and numerous nanowire–nanowire junctions. Figure 2c–h shows the TEM image, SAED pattern, and EDS spectrum of the synthesized SnO₂ nanowires. A lattice spacing of 0.26 nm well matches to the d-spacing (101) of SnO₂ nanowires. The SAED and EDS data also confirmed that SnO₂ nanowires are successfully synthesized. As shown in Figure 2f–h, Au, Sn, and O are distributed uniformly.

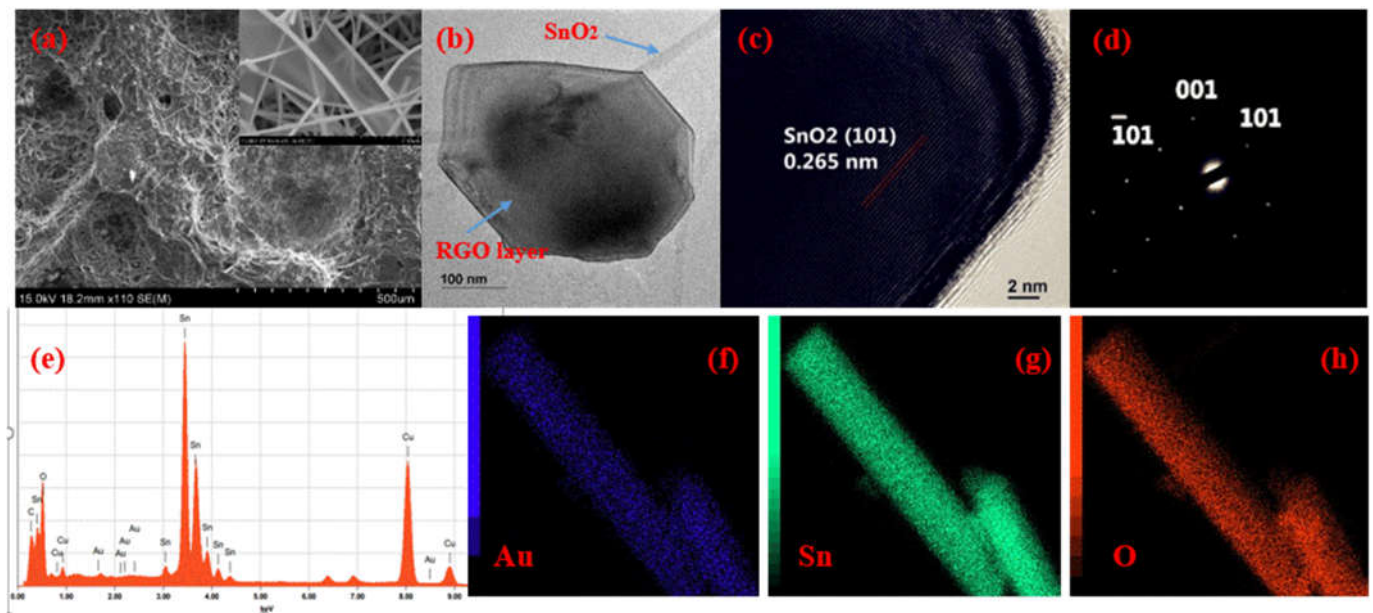


Figure 2. (a) SEM image of the RGO/SnO₂ composite. Inset: the enlargement of a part of the composite; (b) the TEM image of the composite; (c) the HRTEM image of a single-crystalline SnO₂ nanowire; (d) the SAED pattern of the SnO₂ nanowire; (e) the EDS spectra of the SnO₂ nanowire; (f–h) the EDS maps of Au, O, and Sn element of the SnO₂ nanowire.

As mentioned before, due to its large surface-to-volume ratio and excellent electron transport properties, the SnO₂ nanowire has been widely used for toxic gas detection. Commonly, the SnO₂ nanowire growth mechanism corresponds to vapor–liquid–solid (VLS) or vapor–solid (VS) mechanism [17,18]. VLS mechanism has a significant feature

that the metal catalyst would stay at the tip of the nanowire. In this work, EDS mapping indicated Au plays a catalyst and active sites role during the preparation of SnO₂ nanowires. It revealed that the SnO₂ nanowires are mainly composed of O, Sn, and Au. We performed an easy way to show the root of the nanowire to obtain the relationship between Au and nanowires. As shown in Figure 3a, the SnO₂ nanowires were rooted in the Ni foam. The growth parameters are consistent with the SnO₂ nanowires prepared on SiO₂/Si substrate, excluding the changed substrate. We can easily recognize the responding active site for nanowires. It is conducive to speculate about the growth mechanism, which is shown in Figure 3b. Based on the above SnO₂ morphology and structure property analysis, a simple model for the growth mechanism of nanowires is discussed [19].

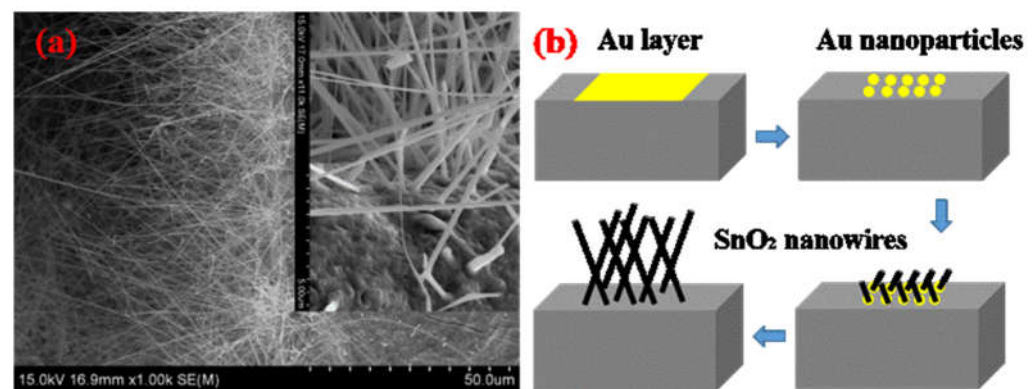
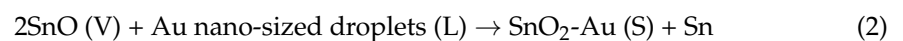
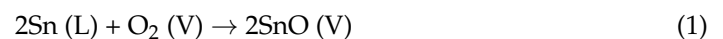


Figure 3. (a) The SEM image of the synthesized SnO₂ nanowires on Ni foam, the inset picture shows the root of the nanowires; (b) the SnO₂ nanowires growth mechanism on SiO₂/Si substrate.

Firstly, because of the low melting point of tin (231.9 °C), the Sn powder would present in the liquid metallic [20] and the liquid tin could react with residual oxygen to yield SnO vapor. Secondly, the Au layer acted as nucleation sites on the SiO₂/Si substrate, while it provided the favored sites for absorption of SnO. Then, the SnO was transformed onto the surface of the Au liquid droplets by the carrying gas. Finally, due to the Au catalyst and SnO decomposition, the SnO₂ nanowires formed immediately [21,22]. Interestingly, there are no metallic Au at the tips of the SnO₂ nanowires but distributed in the whole nanowire as confirmed by the EDS mapping, which is different from the typical characteristics of the VLS growth mechanism.

Figure 4a shows XRD patterns of the GO, RGO, SnO₂ nanowires, and RGO/SnO₂ composite. GO shows a character (002) diffraction peak at $2\theta = 10.83^\circ$. The RGO diffraction peak position is shifted to 23.85° . Hereby, the interlayer distance changed from 0.81 nm to 0.4 nm. It resulted in the decrease in the RGOs' interlayer spacing, which means that oxygen-related chemical groups were significantly removed from GO. The SnO₂ nanowires and RGO/SnO₂ composite matched well with the tetragonal rutile structure (SnO₂, JCPDS No. 41-1445). For RGO/SnO₂ composite, the RGO diffraction peak disappeared, which might be ascribed to the low RGO amount. The significant structural changes occurring from GO to the RGO are also presented in the Raman spectra. In Figure 4b, the Raman spectrum of the GO and RGO samples shows two obvious peaks at 1353 cm^{-1} (D-band) and 1595 cm^{-1} (G-band). Commonly, the G band peak can be ascribed to the E_{2g} vibrational mode of the sp²-bonded carbon atoms [23–25], while the D band peak is ascribed to the defect-induced mode [26,27]. The intensity ratio of the D to G band value of the GO is about 1.049, the increased value of RGO (1.156) suggests a successful chemical reduction of GO. For SnO₂ nanowires and a RGO/SnO₂ composite, the induction of the RGO would not

change the character peaks of the SnO₂ nanowires. The three Raman scattering peaks at 474.8, 633.3, and 773.5 cm⁻¹ correspond to the E_g, A_{1g}, and B_{2g} vibration modes of SnO₂ [28]. Otherwise, the peak at 498 cm⁻¹ is reported to be A_{2u} mode, which has not been detected in bulk SnO₂ [18]. These character peaks further confirm the existence of the SnO₂ and RGO in the RGO/SnO₂ composite, which agrees with the results of XRD characterization.

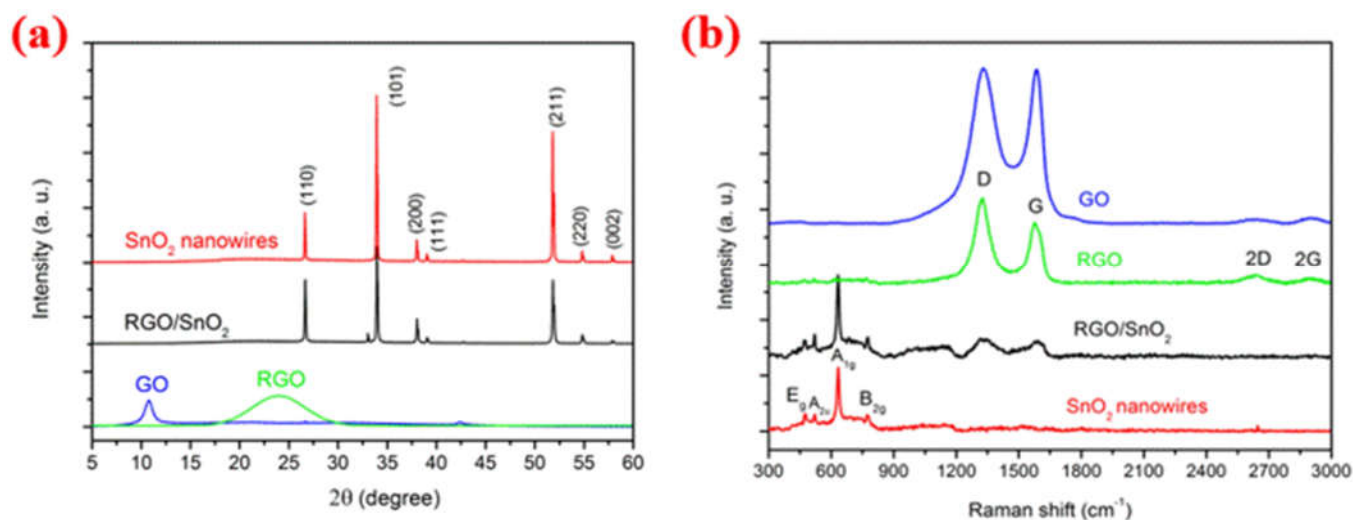


Figure 4. (a) The XRD results; (b) Raman spectra of GO, RGO, RGO/SnO₂ composite, and SnO₂ nanowires.

The sensing properties of SnO₂ nanowires and RGO/SnO₂ composite sensor toward 50 ppm TEA gas at different temperatures are shown in Figure 5a. For the SnO₂ nanowires sensor, the optimal temperature is about 200 °C. Thus, the best gas sensing temperature of the RGO/SnO₂ composite sensor is about 180 °C. RGO/SnO₂ composite sensor had the highest gas response at low temperatures due to the introduction of RGO. As expected, the gas response of the RGO/SnO₂ composite is up to 63.3, which is higher than that of SnO₂ nanowires sensor at the same testing procedures (32 under 50 ppm of TEA gas). Afterward, as the temperature increasing further, the response gradually decreases, which can be attributed to the drop down of equilibrium adsorption capacity [6]. Figure 5b presents dynamic response-recovery properties of the sensor for different TEA gas concentrations ranging from 50 ppb to 200 ppm at 180 °C. The response of the sensor is 2.6 at a TEA concentration of 100 ppb. The sensor got a low detection limit of 50 ppb level. At 180 °C, the sensor response gradually increased with the increase in the gas concentration. When towards 200 ppm, the response is up to 100, showing the excellent gas-sensing property. Figure 5c shows the response time of the sensor is about 10 s. The stability of the RGO/SnO₂ composite sensor is also measured, and the six-cycling dynamic response is shown in Figure 5d. Accordingly, the sensor shows an almost constant response time and response curves for detecting the TEA gas concentration of 1 ppm, showing good stability of the sensor.

The long-term stability and selectivity of gas sensing are fundamental factors in gas detection applications. Figure 6a shows the gas response of the RGO/SnO₂ composite based sensor to 15 dynamic cycles after 30 days at a concentration of 50 ppm. As we can see, the sensor shows good long-term stability and cycling performance. Compared to the fresh sensor, the late sensors' response value had a litter change. As shown in Figure 6b, the sensor responses to different detected gases in a continuous process. The data shows that the response intensity to 1 ppm TEA gas is almost twice as high than the response to the other six gases, even responding to a gas concentration of 100 ppm. In particular, the sensor has a weak response to water, and it shows an anti-water property, which is good for detecting TEA gas regardless of humidity in real situations.

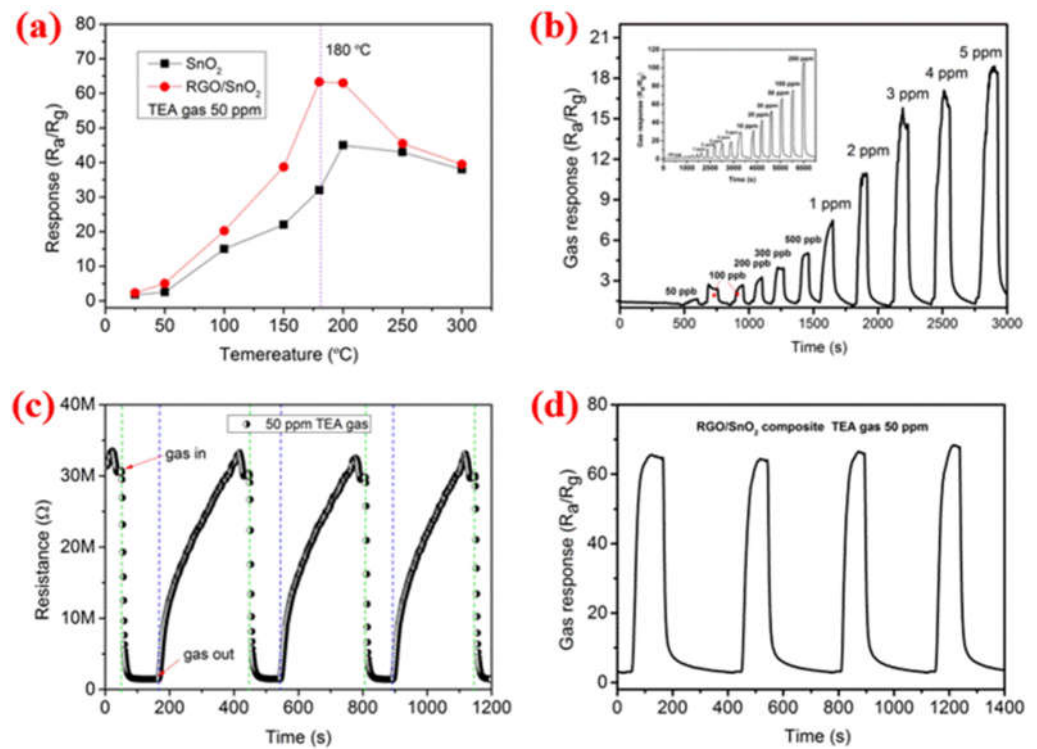


Figure 5. (a) Sensor response of the SnO₂ nanowires and RGO/SnO₂ composite to 50 ppm TEA gas at different working temperatures; (b) the dynamic gas response at different TEA gas concentrations ranging from 50 ppb to 200 ppm; (c) sensor response time toward 50 ppm TEA gas at 180 °C; (d) the four dynamic gas-sensing response cycles at 180 °C.

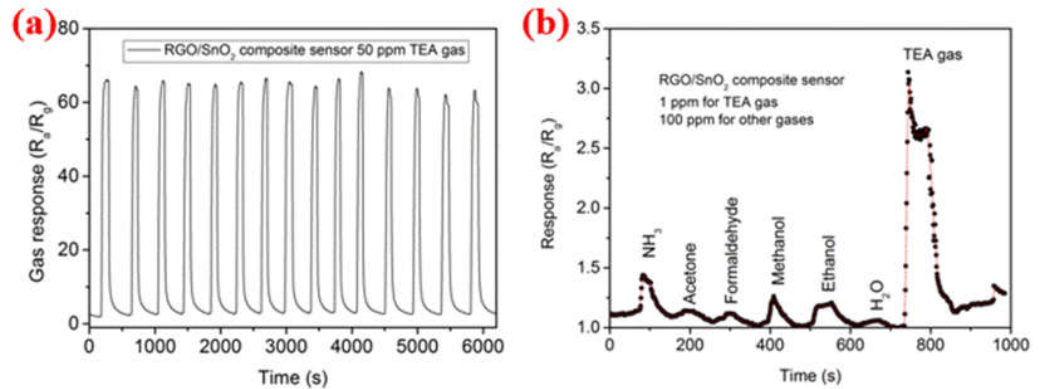


Figure 6. (a) The gas sensing stability of the sensor after 30 days; (b) the gas selectivity of the sensor to six different gases at a concentration of 1 ppm.

Generally, it is well known that the one-dimensional SnO₂ nanowire has a large surface-to-volume ratio and constant carrier screening length, which facilitates more rapid and high-efficient adsorption for improving the gas response [29]. Thus, due to the intertwined and irregular stacking of SnO₂ nanowires, the material resistance is as high as hundreds of megaohms (M Ω), making it difficult to integrate with existing electronic systems. The RGO could help improve the conductivity of metal oxide and promote the transfer of electrons. When the composite material meets air, oxygen would be adsorbed, and then would react with the free electrons to ionize oxygen into oxygen species (O^{-2} , O^{2-} , and O^{-}) on the surface of SnO₂ nanowires and RGO [30]. The depletion layer formed as shown in Figure 7a. As exposure to targeted gas, the captured electrons are released as reacting with the existing oxygen ions, reducing the thickness of the depletion layer and the resistance would be minimized. The gas response is largely enhanced. Wang et al. demonstrated the preparation of ZnO/SnO₂ heterostructure on RGO layer, and found promising sensing behavior upon

NO₂ exposure even at room temperature. They presented that the heterostructure could offer effective electronic interaction and high transfer efficiency of charges at the interface, which help to adsorb oxygen for enhancing the gas response [31]. So, in Figure 7b, we showed the current–voltage characteristic relationship of the RGO/SnO₂ composite gas sensor in air and after exposure to 50 ppm TEA gas, respectively. After being exposed to targeted gas, the current proudly increased because of the changed conductivity after surface reactions between TEA gas and adsorption oxygen. The following reaction can be depicted as follows [32]:

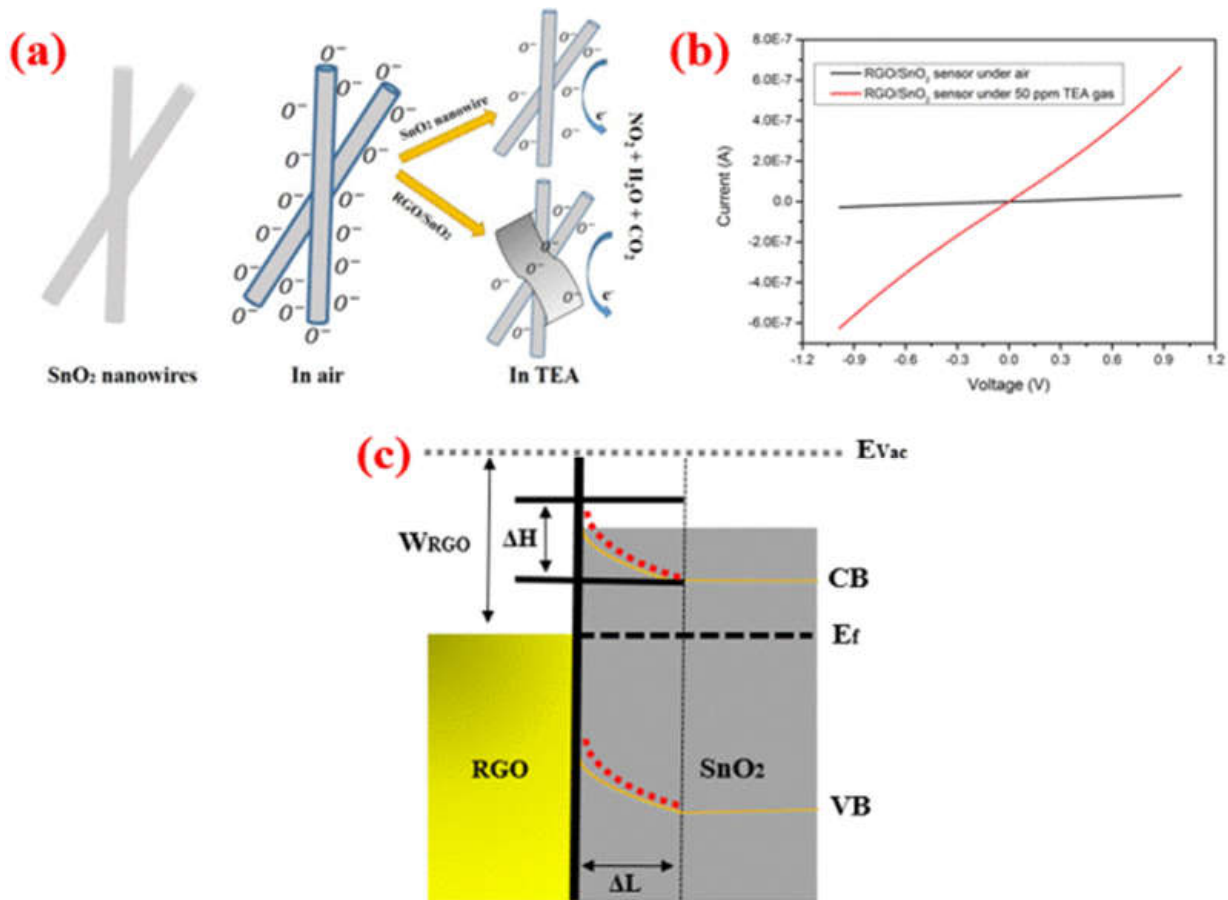
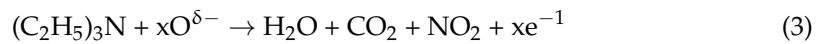


Figure 7. (a) Schematic of the RGO/SnO₂ composite gas-sensing mechanism; (b) the current–voltage characteristic relationship of the RGO/SnO₂ composite gas sensor in air and after exposure to 50 ppm TEA gas, respectively; (c) energy band diagram of the RGO/SnO₂ composite.

The gas-sensing mechanism of RGO/SnO₂ heterostructure-based sensors can be concluded. Notably, RGO could play a significant role and provide reactive centers for adsorption, which facilitates rapid electrons transformation between targeted gas and SnO₂. SnO₂, as a promising and mature gas-sensing material, could also promote effective charge transfer and oxygen adsorption. Therefore, when the RGO/SnO₂ composite encounters TEA gas, the energy band bending would happen until balance, as depicted in Figure 7c. The electron movement will start flowing from RGO to SnO₂. So, when encountering the targeted gas, the adsorbed process was happening at the interface, a small change in the potential barrier (E) would contribute to a large resistance change of the material. The resistance is related to the height of the potential barrier, which is followed by the equation [30]:

$$R = R_0 \exp(qE/kT) \tag{4}$$

Generally, R_0 is the initial resistance, q is the electron charge, E is the height of the potential energy barrier, k is Boltzmann's constant, T is the temperature, and R is the overall resistance of the material. So, based on the above results, the RGO/SnO₂ heterostructure enhanced the gas-sensing performance and provided a reliable strategy to obtain the highly sensitive.

4. Conclusions

In summary, the crystalline SnO₂ nanowires are synthesized by a simple thermal evaporation method. We also presented a coating technology to realize RGO/SnO₂ heterostructure. When the TEA gas concentration is 50 ppm, the gas response is raised to 63.3, and it showed an excellent dynamic response with a high stability at 180 °C. A lower detection limit of 50 ppb level is achieved. Compared to SnO₂ nanowires, the sensing performance of the RGO/SnO₂ heterostructure-based sensor is greatly enhanced, which can be ascribed to the RGO and the heterostructure. This heterostructure engineering poses an easy and repeatable way for achieving highly sensitive performance.

Author Contributions: Formal analysis, investigation, writing—original draft preparation. R.P.; writing—review and editing, X.Z. and Y.L.; visualization, Z.Y.; supervision, L.C. All authors have read and agreed to the published version of the manuscript.

Funding: This work was supported by the Shandong Provincial Science and Technology Major Project (2019GGX101029) and the National Science Foundation of Shandong Province (ZR2017BEM049).

Institutional Review Board Statement: Not applicable.

Informed Consent Statement: Not applicable.

Data Availability Statement: Not applicable.

Acknowledgments: The authors thank the technical supporting from the Research Center for Carbon Nanomaterials, Shandong University.

Conflicts of Interest: The authors declare no conflict of interest.

References

1. Wang, D.; Chu, X.; Gong, M. Gas-Sensing Properties of Sensors Based on Single-Crystalline SnO₂ Nanorods Prepared by a Simple Molten-Salt Method. *Sens. Actuators B Chem.* **2006**, *117*, 183–187. [[CrossRef](#)]
2. Shi, L.; Naik, A.J.; Goodall, J.B.; Tighe, C.; Gruar, R.; Binions, R.; Parkin, I.; Darr, J. Highly Sensitive ZnO Nanorod-and Nanoprism-Based NO₂ Gas Sensors: Size and Shape Control Using a Continuous Hydrothermal Pilot Plant. *Langmuir* **2013**, *29*, 10603–10609. [[CrossRef](#)]
3. Tomer, V.K.; Devi, S.; Malik, R.; Nehra, S.; Duhan, S. Highly Sensitive and Selective Volatile Organic Amine (VOA) Sensors Using Mesoporous WO₃-SnO₂ Nanohybrids. *Sens. Actuators B Chem.* **2016**, *229*, 321–330. [[CrossRef](#)]
4. Barthod-Malat, B.; Hauguel, M.; Behloul, K.; Grisel, M.; Savary, G. Influence of the Compression Molding Temperature on VOCs and Odors Produced from Natural Fiber Composite Materials. *Coatings* **2023**, *13*, 371. [[CrossRef](#)]
5. Lazau, C.; Nicolaescu, M.; Orha, C.; Pop, A.; Căprărescu, S.; Bandas, C. In Situ Deposition of Reduced Graphene Oxide on Ti Foil by a Facile, Microwave-Assisted Hydrothermal Method. *Coatings* **2022**, *12*, 1805. [[CrossRef](#)]
6. Zhu, L.Y.; Miao, X.Y.; Ou, L.X.; Mao, L.W.; Yuan, K.; Sun, S.; Devi, A.; Lu, H.L. Heterostructured α -Fe₂O₃@ZnO@ZIF-8 Core-Shell Nanowires for a Highly Selective MEMS-Based ppb-Level H₂S Gas Sensor System. *Small* **2022**, *18*, 2204828. [[CrossRef](#)] [[PubMed](#)]
7. Kim, T.; Cho, W.; Kim, B.; Yeom, J.; Kwon, Y.M.; Baik, J.M.; Kim, J.J.; Shin, H. Batch Nanofabrication of Suspended Single 1D Nanoheaters for Ultralow-Power Metal Oxide Semiconductor-Based Gas Sensors. *Small* **2022**, *18*, 2204078. [[CrossRef](#)]
8. Yu, Y.-T.; Dutta, P. Examination of Au/SnO₂ Core-Shell Architecture Nanoparticle for Low Temperature Gas Sensing Applications. *Sens. Actuators B Chem.* **2011**, *157*, 444–449. [[CrossRef](#)]
9. Yu, Q.; Zhu, J.; Xu, Z.; Huang, X. Facile Synthesis of α -Fe₂O₃@SnO₂ Core-Shell Heterostructure Nanotubes for High Performance Gas Sensors. *Sens. Actuators B Chem.* **2015**, *213*, 27–34. [[CrossRef](#)]
10. Wang, B.; Zhu, L.; Yang, Y.; Xu, N.; Yang, G. Fabrication of a SnO₂ Nanowire Gas Sensor and Sensor Performance for Hydrogen. *J. Phys. Chem. C* **2008**, *112*, 6643–6647. [[CrossRef](#)]
11. Zou, Y.; Chen, S.; Sun, J.; Liu, J.; Che, Y.; Liu, X.; Zhang, J.; Yang, D. Highly Efficient Gas Sensor Using a Hollow SnO₂ Microfiber for Triethylamine Detection. *ACS Sens.* **2017**, *2*, 897–902. [[CrossRef](#)] [[PubMed](#)]
12. Lipatov, A.; Varezchnikov, A.; Wilson, P.; Sysoev, V.; Kolmakov, A.; Sinitiskii, A. Highly Selective Gas Sensor Arrays Based on Thermally Reduced Graphene Oxide. *Nanoscale* **2013**, *5*, 5426–5434. [[CrossRef](#)] [[PubMed](#)]

13. Song, Z.; Wei, Z.; Wang, B.; Luo, Z.; Xu, S.; Zhang, W.; Yu, H.; Li, M.; Huang, Z.; Zang, J. Sensitive Room-Temperature H₂S Gas Sensors Employing SnO₂ Quantum Wire/Reduced Graphene Oxide Nanocomposites. *Chem. Mater.* **2016**, *28*, 1205–1212. [[CrossRef](#)]
14. Zhang, S.; Zhang, B.; Sun, G.; Li, Y.; Zhang, B.; Wang, Y.; Cao, J.; Zhang, Z. One-Step Synthesis of Ag/SnO₂/rGO Nanocomposites and Their Trimethylamine Sensing Properties. *Mater. Res. Bull.* **2019**, *114*, 61–67. [[CrossRef](#)]
15. Mao, S.; Yu, K.; Cui, S.; Bo, Z.; Lu, G.; Chen, J. A New Reducing Agent to Prepare Single-Layer, High-Quality Reduced Graphene Oxide for Device Applications. *Nanoscale* **2011**, *3*, 2849–2853. [[CrossRef](#)] [[PubMed](#)]
16. Peng, R.; Li, Y.; Chen, J.; Si, P.; Feng, J.; Zhang, L.; Ci, L. Reduced Graphene Oxide Wrapped Au@ ZnO Core-Shell Structure for Highly Selective Triethylamine Gas Sensing Application at a Low Temperature. *Sens. Actuators A Phys.* **2018**, *283*, 128–133. [[CrossRef](#)]
17. Duan, X.; Lieber, C.M. General Synthesis of Compound Semiconductor Nanowires. *Adv. Mater.* **2000**, *12*, 298–302. [[CrossRef](#)]
18. Wang, J.; Liu, D.; Yan, X.; Yuan, H.; Ci, L.; Zhou, Z.; Gao, Y.; Song, L.; Liu, L.; Zhou, W. Growth of SnO₂ Nanowires with Uniform Branched Structures. *Solid State Commun.* **2004**, *130*, 89–94. [[CrossRef](#)]
19. Li, Y.; Peng, R.; Xiu, X.; Zheng, X.; Zhang, X.; Zhai, G. Growth of SnO₂ Nanoparticles via Thermal Evaporation Method. *Superlattices Microstruct.* **2011**, *50*, 511–516. [[CrossRef](#)]
20. Sun, Q.; Yang, M.; Zeng, G.; Li, J.; Hu, Z.; Li, D.; Wang, S.; Si, P.; Tian, Y.; Ci, L. Insights into the Potassium Ion Storage Behavior and Phase Evolution of a Tailored Yolk–Shell SnSe@ C Anode. *Small* **2022**, *18*, 2203459. [[CrossRef](#)]
21. Mohammad-Yousefi, S.; Rahbarpour, S.; Ghafoorifard, H. Describing the Effect of Ag/Au Modification on Operating Temperature and Gas Sensing Properties of Thick Film SnO₂ Gas Sensors by Gas Diffusion Theory. *Mater. Chem. Phys.* **2019**, *227*, 148–156. [[CrossRef](#)]
22. Bahrami, B.; Khodadadi, A.; Kazemeini, M.; Mortazavi, Y. Enhanced CO Sensitivity and Selectivity of Gold Nanoparticles-Doped SnO₂ Sensor in Presence of Propane and Methane. *Sens. Actuators B Chem.* **2008**, *133*, 352–356. [[CrossRef](#)]
23. Sharma, N.; Sharma, V.; Jain, Y.; Kumari, M.; Gupta, R.; Sharma, S.; Sachdev, K. Synthesis and Characterization of Graphene Oxide (GO) and Reduced Graphene Oxide (rGO) for Gas Sensing Application. *Macromol. Symp.* **2017**, *376*, 1700006. [[CrossRef](#)]
24. Sun, Q.; Li, J.; Yang, M.; Wang, S.; Zeng, G.; Liu, H.; Cheng, J.; Li, D.; Wei, Y.; Si, P.; et al. Carbon Microstructure Dependent Li-Ion Storage Behaviors in SiOx/C Anodes. *Small* **2023**, *2023*, 2300759. [[CrossRef](#)]
25. Wang, S.; Tian, Y.; Wang, C.; Hang, C.; Huang, Y.; Liao, C. Chemical and Thermal Robust Tri-Layer rGO/Ag NWs/GO Composite Film for Wearable Heaters. *Compos. Sci. Technol.* **2019**, *174*, 76–83. [[CrossRef](#)]
26. Sieradzka, M.; Ślusarczyk, C.; Biniś, W.; Fryczkowski, R. The Role of the Oxidation and Reduction Parameters on the Properties of the Reduced Graphene Oxide. *Coatings* **2021**, *11*, 166. [[CrossRef](#)]
27. Sun, Q.; Li, J.; Hao, C.; Ci, L. Focusing on the Subsequent Coulombic Efficiencies of SiOx: Initial High-Temperature Charge after Over-Capacity Prelithiation for High-Efficiency SiOx-Based Full-Cell Battery. *ACS Appl. Mater. Interfaces* **2022**, *14*, 14284–14292. [[CrossRef](#)]
28. Sun, S.; Meng, G.; Zhang, G.; Gao, T.; Geng, B.; Zhang, L.; Zuo, J. Raman Scattering Study of Rutile SnO₂ Nanobelts Synthesized by Thermal Evaporation of Sn Powders. *Chem. Phys. Lett.* **2003**, *376*, 103–107. [[CrossRef](#)]
29. Asadzadeh, M.Z.; Köck, A.; Popov, M.; Steinhauer, S.; Spitaler, J.; Romaner, L. Response Modeling of Single SnO₂ Nanowire Gas Sensors. *Sens. Actuators B Chem.* **2019**, *295*, 22–29. [[CrossRef](#)]
30. Xu, Q.; Ju, D.; Zhang, Z.; Yuan, S.; Zhang, J.; Xu, H.; Cao, B. Near Room-Temperature Triethylamine Sensor Constructed with CuO/ZnO PN Heterostructural Nanorods Directly on Flat Electrode. *Sens. Actuators B Chem.* **2016**, *225*, 16–23. [[CrossRef](#)]
31. Wang, Z.; Gao, S.; Fei, T.; Liu, S.; Zhang, T. Construction of ZnO/SnO₂ Heterostructure on Reduced Graphene Oxide for Enhanced Nitrogen Dioxide Sensitive Performances at Room Temperature. *ACS Sens.* **2019**, *4*, 2048–2057. [[CrossRef](#)] [[PubMed](#)]
32. Liu, X.; Zhao, K.; Sun, X.; Zhang, C.; Duan, X.; Hou, P.; Zhao, G.; Zhang, S.; Yang, H.; Cao, R. Rational Design of Sensitivity Enhanced and Stability Improved TEA Gas Sensor Assembled with Pd Nanoparticles-Functionalized In₂O₃ Composites. *Sens. Actuators B Chem.* **2019**, *285*, 1–10. [[CrossRef](#)]

Disclaimer/Publisher's Note: The statements, opinions and data contained in all publications are solely those of the individual author(s) and contributor(s) and not of MDPI and/or the editor(s). MDPI and/or the editor(s) disclaim responsibility for any injury to people or property resulting from any ideas, methods, instructions or products referred to in the content.